

Evidence that seismic anisotropy captures upstream palaeo ice fabric: Implications on present day deformation at Whillans Ice Stream, Antarctica

Justin LEUNG¹, Thomas Samuel HUDSON^{1,2}, John-Michael KENDALL¹, Grace BARCHECK³

¹*Department of Earth Sciences, University of Oxford, Oxford, UK*

²*Department of Earth and Planetary Sciences, ETH Zurich, 8092 Zurich, Switzerland*

³*Department of Earth and Atmospheric Sciences, Cornell University, Ithaca, NY, USA*

Correspondence: Justin Leung <justin.leung@earth.ox.ac.uk>

ABSTRACT. Understanding deformation and slip at ice streams, which are responsible for 90 % of Antarctic ice loss, is vital for accurately modelling large-scale ice flow. Ice crystal orientation fabric (COF) has a first-order effect on ice stream deformation. For the first time, we use shear-wave splitting (SWS) measurements of basal icequakes at Whillans Ice Stream (WIS), Antarctica, to determine a shear-wave anisotropy with an average delay time of 7 ms and fast S-wave polarisation (φ) of 29.3°. The polarisation is expected to align perpendicular to ice flow, whereas our observation is oblique to the current ice flow direction ($\sim 280^\circ$). This suggests that ice at WIS preserves upstream fabric caused by palaeo-deformation developed over at least the past 450 years, which provides evidence of the concept of Microstructural Fading Memory. Our results imply that changes in the shape of WIS occur on timescales shorter than COF re-equilibration. The “palaeo-fabric” can somewhat control present-day ice flow, which we suggest may somewhat contribute to the long-term slowdown at WIS. Our findings suggest that seismic anisotropy can provide information on past ice sheet dynamics, and how past ice dynamics can play a role in controlling current deformation.

26 INTRODUCTION

27 Despite ice streams spanning only 10 % of Antarctica’s surface area, they are responsible for 90 % of
28 Antarctic ice loss (Morgan and others, 1982). Therefore, studying ice stream rheology is important for
29 understanding Antarctica’s contribution to sea-level rise. One source of uncertainty in ice stream dynamics
30 is the effect of ice fabrics on rheology, where ice with a crystal oriented fabric (COF) can be ten times
31 weaker in shear in a particular direction relative to isotropic ice (Budd and Jacka, 1989; Pimienta and
32 others, 1987). Glacial ice is formed of anisotropic grains with hexagonal crystalline symmetry, such that
33 the viscosity along the basal plane of ice (normal to c-axis) is sixty times less than that perpendicular to
34 it (Duval and others, 1983). Under stress, the c-axes in a bulk polycrystalline ice mass can rotate to form
35 an ice COF over timescales of hundreds of years, which can change in response to the stress it encounters
36 (Azuma, 1994). Hence, understanding ice COF provides insight on past deformation history and how it
37 might influence future ice flow.

38 Most glacial ice COF measurements are taken from microstructural analyses of ice core samples. How-
39 ever, these are usually measured from stable or slow-moving regions of ice sheets, and cannot provide much
40 information of the physical processes in fast-deforming regions (Fan and others, 2021; Llorens and others,
41 2022). In contrast, seismic anisotropy measurements can be used to deduce ice COF properties over large
42 areas in different ice settings, including ice streams (Smith and others, 2017). Therefore, seismic anisotropy
43 can provide insight in these key fast-flowing regions, which can inform models of ice-sheet dynamics.

44 Whillans Ice Stream (WIS) is a major ice stream in West Antarctica that flows into the Ross Sea
45 embayment (see Figure 1; Picotti and others, 2015). The downstream portion of WIS is known as Whillans
46 Ice Plain (WIP), and it flows at a speed of over 300 metres per year, with stable sliding of the ice stream
47 punctuated 1-2 times daily by sudden unstable sliding motion during 30-minute slip events that also
48 produce high frequency icequakes and tremor (Barcheck and others, 2018; Bindschadler and others, 2003;
49 Winberry and others, 2013). Long-term slowdown of the ice stream can be seen, with longer periods of
50 quiescence between slip events over time, suggesting possibility of future stagnation (Winberry and others,
51 2014). WIS is an excellent area to study basal seismicity given that seismic and global navigation satellite
52 system data have been collected over recent decades at numerous sites to study its stick-slip cycle (e.g.
53 Barcheck and others, 2020; Pratt and others, 2014; Walter and others, 2011, 2015; Winberry and others,
54 2009, 2011) and basal hydrologic cycle (e.g. Fricker and Scambos, 2009; Siegfried and others, 2016).

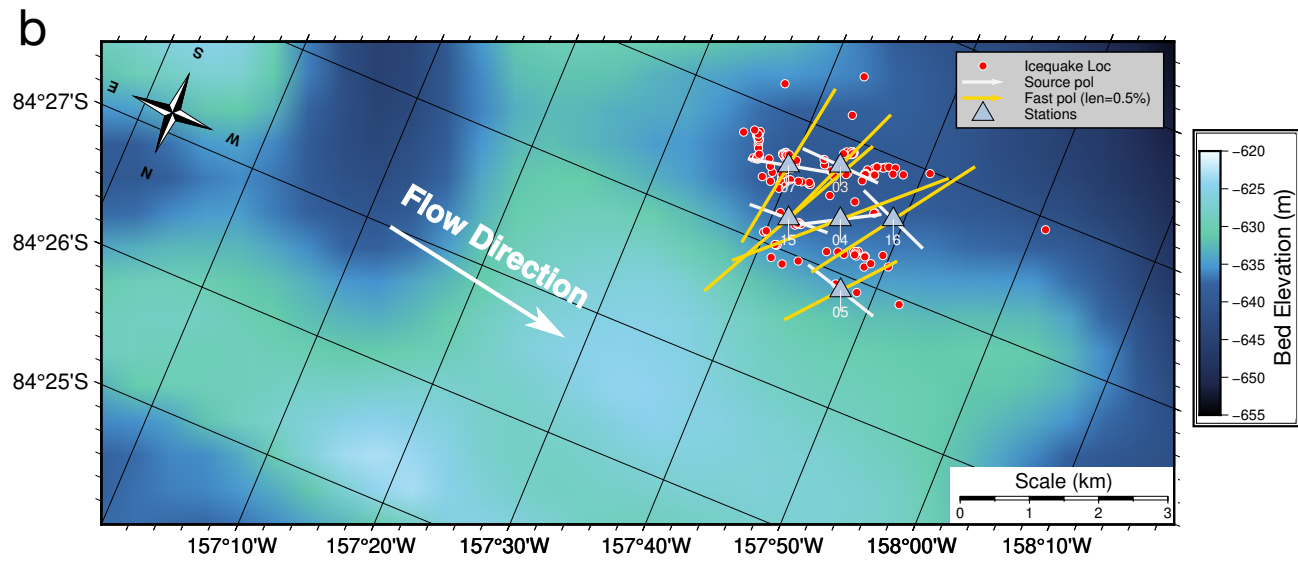
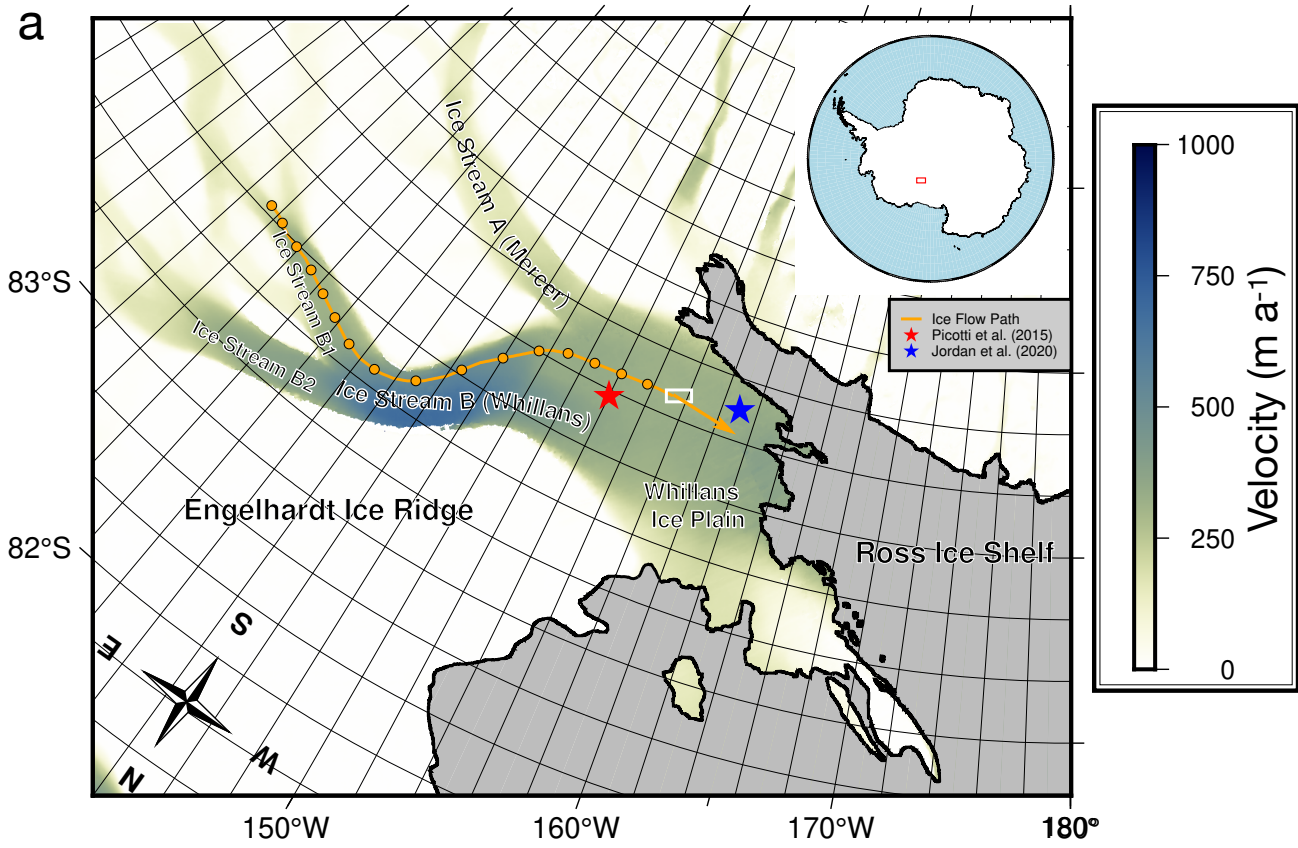


Fig. 1. Stereographic maps showing Whillans Ice Stream (WIS) and study location. (a) Regional map of the WIS. The grounding line is marked in the thick black line, and the grey shaded areas mark regions of floating ice. The blue and red star show the study site locations of Jordan and others (2020) and Picotti and others (2015) respectively. The orange line outlines the upstream flow path of the ice at our study site location, assuming current flow velocities, with orange points marking the locations at intervals of 50 years (see supplementary information for flow path calculation). The background colour map shows the ice flow velocity obtained from MEaSURES InSAR-Based Antarctica Ice Velocity Map, Version 2 (Rignot and others, 2017). The study area in (b) is outlined by the white box. (b) Detailed map of the study region. Stations are marked as blue triangles, and icequake locations are shown by red scatter points. Gold lines show the fast S-wave polarisation direction, with the length of the line representing the strength of anisotropy. White lines show the source polarisations for each event, as estimated from recorded shear waves. Dominant ice flow direction (280°) is indicated by the large white arrow. The background

56 colour map shows the bed elevation (Morlighem, 2022).

57 There are currently few ice COF observations for the entire ice column at WIS. Picotti and others (2015)
 58 used active seismic sources to suggest an azimuth-independent vertically transverse isotropic fabric (VTI)
 59 at WIS, with a focus on the top 200 metres. Conversely, Jordan and others (2020) used electromagnetic
 60 methods to argue that the c-axes orient parallel to flow at WIS by polarimetric radar sounding that
 61 measured the top 400 metres of WIS (see Figure 1 for locations). Here, we provide the first seismic
 62 anisotropy measurements from shear-wave splitting of basal icequakes of the entire ice column at Whillans
 63 Ice Stream.

64 METHODOLOGY

65 This study uses 319 icequakes recorded between January 20th and February 27th, 2014 by six seismometers
 66 at Whillans Ice Plain, Antarctica, part of a network active between 2012 to 2018 (Barcheck and others,
 67 2020; Schwartz, 2012). The ice at the study site is between 690 and 710 m thick (Barcheck and others, 2020)
 68 and moving at $\sim 370 \text{ m a}^{-1}$ (Morlighem, 2022). Since horizontal orientation of the instruments is important
 69 for studying seismic anisotropy, we verified the orientation of these instruments using a teleseismic event.
 70 We performed a manual search for icequakes focused within the duration of bidaily slip events at WIS,
 71 described in Barcheck and others (2021). Icequake arrival times are picked manually and are located using
 72 NonLinLoc, a probabilistic non-linear earthquake location algorithm (Lomax and others, 2000). Only
 73 icequakes originating at the bed of the ice stream are of interest for measuring total anisotropy in the ice
 74 column, therefore icequakes with a source depth shallower than 400 metres are removed. Each icequake is

75 filtered by a 10-100 Hz bandpass filter, based on the dominant source spectra of the icequakes (see Figure
 76 S1). Seismic anisotropy is analysed on the horizontal (north and east) components because a ~ 100 m thick
 77 firn layer refracts the ray path of icequakes to near-vertical incidence at the surface (Picotti and others,
 78 2015).

79 Shear-wave splitting (SWS) analysis is conducted using the python package SWSPy (Hudson and
 80 others, 2023), based on the approach of Wuestefeld and others (2010). It can be summarised as follows:
 81 First, a range of analysis time windows are defined because SWS measurements are sensitive to window
 82 lengths (Teanby and others, 2004). Second, a grid search is performed over fast shear-wave polarisation
 83 of $-90^\circ < \varphi \leq 90^\circ$ and delay times between fast and slow S-waves of $0 \leq \delta t \leq 0.1$ for each window, such
 84 that $\varphi = 0$ represents a fast shear-wave polarisation in the north (and south) direction. The splitting
 85 parameters, φ and δt , associated with the minimum second eigenvalue of the S-wave covariance matrix
 86 that best linearize particle motion, describe the anisotropy observed along a given source-receiver ray path.
 87 Third, density-based cluster analysis is performed on all optimal φ and δt values, such that the optimal
 88 φ and δt values are obtained from the most stable cluster with minimum variance in φ and δt (Ester and
 89 others, 1996; Teanby and others, 2004). The source polarisation is then calculated by taking the azimuth
 90 of the largest eigenvalue of the covariance matrix of the linearised waveforms (Walsh and others, 2013).

91 A well-constrained result after SWS correction is defined as satisfying the following four requirements:
 92 (1) the particle motion (see Figure 2c) becomes approximately linear after removing splitting using the
 93 optimal SWS parameters, (2) the error surface (see Figure 2f) has a unique, well-constrained solution, (3)
 94 splitting parameters (φ and δt) are stable (see Figure 2e) throughout different clusters, and (4) the quality
 95 factor Q_w is larger than 0.7. Q_w measures the robustness of the splitting measurement, and it is calculated
 96 by comparing the results from the eigenvalue method of Silver and Chan (1991) to the cross-correlation
 97 method of Menke and Levin (2003). A value of $Q_w = 1$ signifies a perfect match between the two methods,
 98 $Q_w = -1$ a good null result, and $Q_w = 0$ a poor result (Wuestefeld and others, 2010).

The strength of anisotropy (δV), or the difference between fast and slow S-wave velocities, can be
 quantified by the change in velocity, derived from the delay time (δt):

$$\delta V = (V \times \delta t \times 100)/r, \quad (1)$$

99 where $V = 1944 \text{ m s}^{-1}$ is the average isotropic shear-wave speed (Smith and others, 2017) and r the
 100 source-receiver distance.

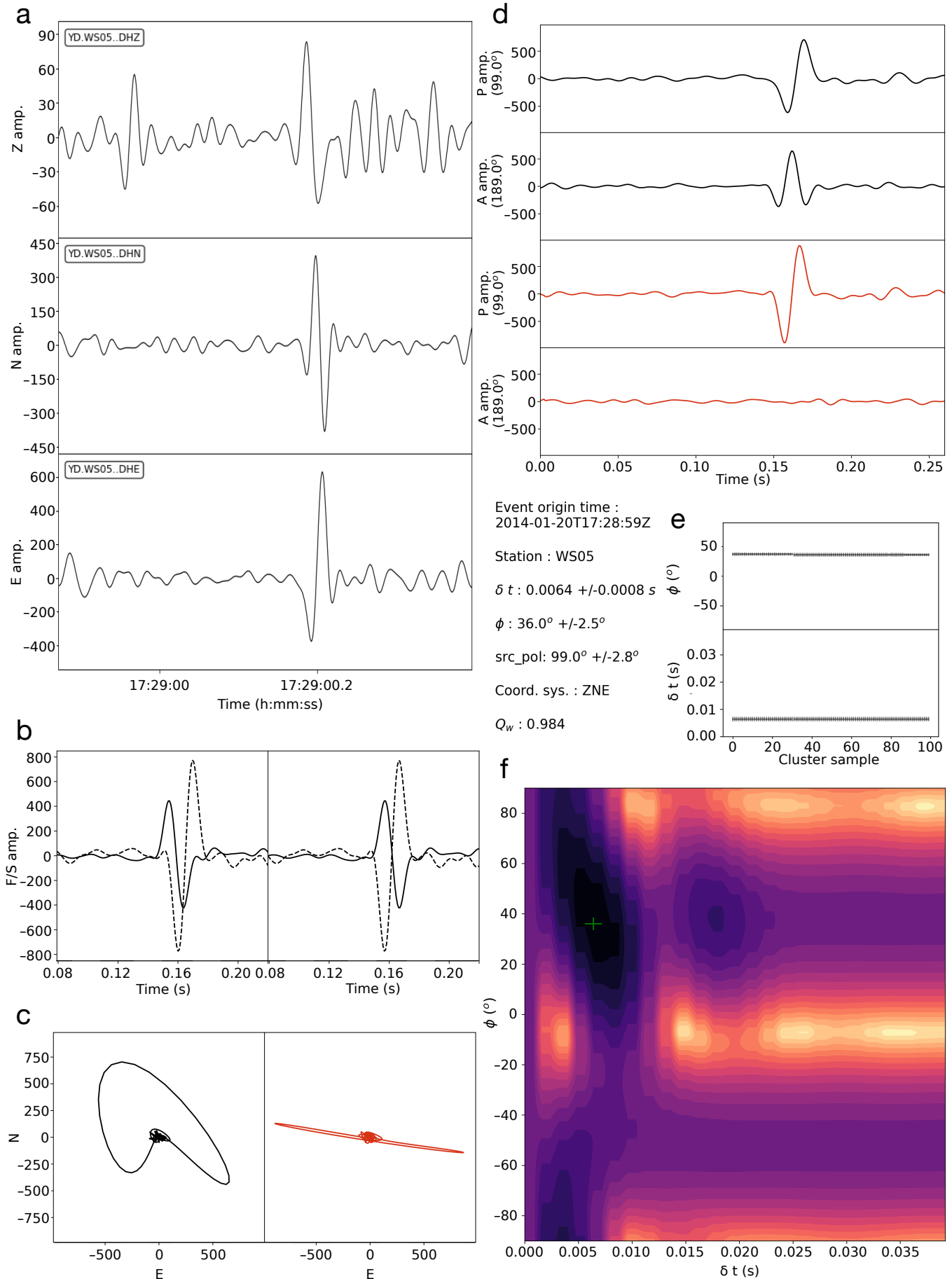


Fig. 2. An example of a well-constrained shear-wave splitting event. (a) Icequake signal before correction in the vertical, north and east component. (b) The waveforms before (left) and after (right) SWS correction, plotted in the fast (black line) and slow (dotted) directions. (c) Horizontal (north and east) particle motion before (left) and after (right) SWS correction. (d) Particle motion of icequakes in the source polarisation (P) and the perpendicular azimuth (A) before (top two) and after (bottom two) correction. (e) Optimal φ and δt for different cluster sizes. A good splitting measurement should have constant φ and δt values independent of cluster size. (f) Error surface plotted on φ vs δt . Larger errors are represented with brighter colours, and smaller errors with darker colours. The optimal φ and δt and its uncertainties are shown with the green symbol.

RESULTS

80 results from 70 events fulfill the aforementioned four criteria, and therefore are chosen for further analysis. The fast S-wave polarisation φ and source polarisation of these events are plotted as polar histograms in Figure 3. For a double-couple icequake source associated with ice slip at the bed, S-wave source polarisation is aligned with the direction of slip (Hudson and others, 2020). One might typically expect the average S-wave source polarisation to align approximately with ice flow direction. Most source polarisation measurements lie approximately in the east-west direction with an average of $264^\circ\text{N} \pm 22^\circ$ (see Figure 3a), which is in agreement with the Whillans Ice Stream’s flow direction of $280^\circ\text{N} \pm 2^\circ$ (Rignot and others, 2017).

The average delay time for these results is 7.1 ms and ranges from 1.6 ms to 19.2 ms. The average strength of anisotropy, δV , is $\sim 1.5\%$, with a maximum of 2.8%. This is below the maximum directional variation in S-wave velocities of single ice crystals of 12% (Lutz and others, 2020).

The shear-wave splitting measurements have an overall mean fast S-wave direction (φ) of $29.3^\circ\text{N} \pm 18^\circ$ (see Figure 3b). The uncertainty in this result is defined as one standard deviation, likely representing an upper estimate of uncertainty in the result that could be caused by temporal variations in φ (see Figure S2). Individual receivers generally have mean φ that fall within a range of 22.4°N to 47.0°N (see Figure 1b), with the exception of station WS07, which has a mean φ of 9.1°N (see label 07, Figure 1b). Ice core studies (Lipenkov and others, 1989; Wang and others, 2002; Weikusat and others, 2017) and seismic anisotropy studies (Kufner and others, 2023; Smith and others, 2017) have found that regions of longitudinal extension, such as ice divides and ice streams, have a vertical girdle fabric. In such fabrics, φ is found to be perpendicular to the ice flow direction (Harland and others, 2013). Based on ice flow direction derived from InSAR (Rignot and others, 2017) and the source polarisation data in Figure 3a, one would expect φ

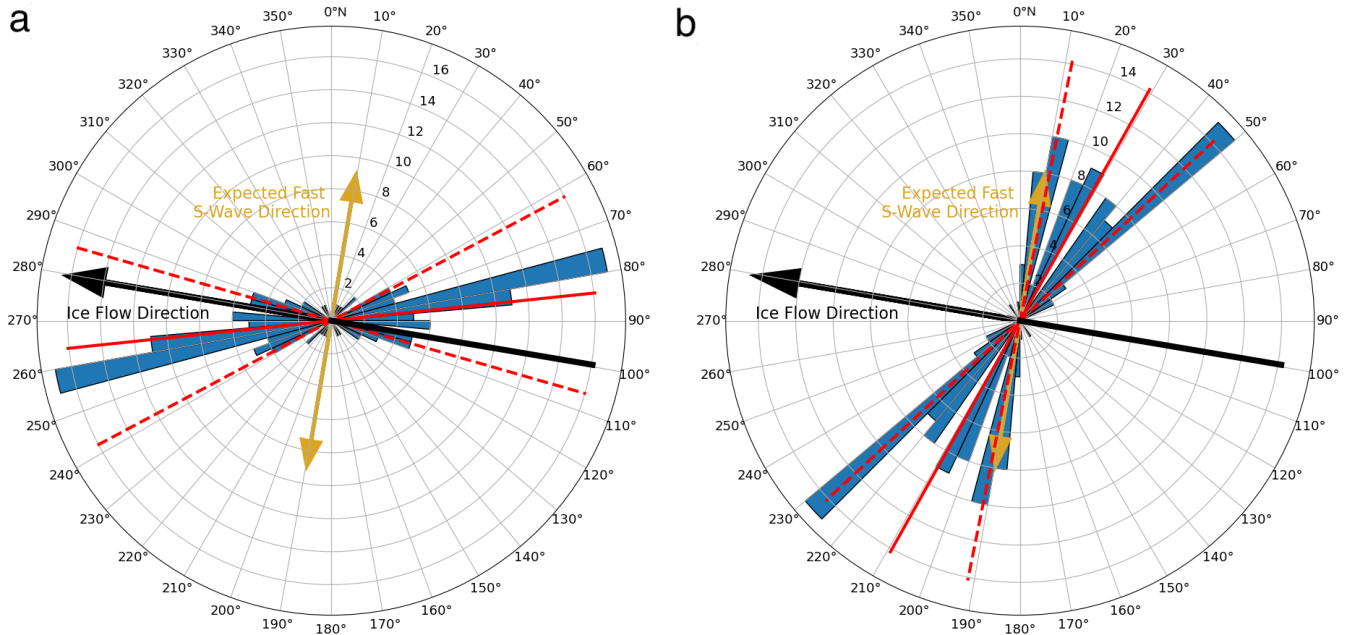


Fig. 3. Rose diagrams of (a) source polarisations and (b) fast S-wave directions for all the 80 SWS measurements. The solid and dotted red lines indicate the averages and uncertainties respectively. The gold arrows on both diagrams indicate the expected fast S-wave direction based on ice flow direction, which are shown as black arrows (see main text for further details). Method for estimating uncertainty is included in the supplementary information.

125 $\sim 10^\circ\text{N}$ at the Whillans study site (golden arrow, Figure 3). However, the mean φ we observe of 29.3°N
 126 $\pm 18^\circ$ is oblique to this expected fast S-wave direction of $\sim 10^\circ\text{N}$, even after accounting for uncertainty.
 127 A t-test shows that the 95 % confidence interval of the fast S-wave directions lies in between 25.3°N and
 128 33.3°N (assuming that the distribution of fast S-wave directions in the data is Gaussian), confirming our
 129 confidence in this obliquity.

130 DISCUSSION

131 Possible origins of an ice COF with an oblique fast S-wave direction

132 Our results suggest that the ice COF at Whillans Ice Stream (WIS) is oriented oblique, rather than
 133 perpendicular, to the ice flow direction. This obliqueness suggests one of two hypotheses: either that the
 134 local strain at our study site acts oblique to ice flow; or that the ice COF at WIS is the result of preservation
 135 of historic deformation upstream of the study site.

136 Regarding the first hypothesis, a possible reason for extension oblique to ice flow is the differential ice
 137 flux between the two tributaries of Whillans Ice Plain (WIP) across a suture zone. The study site is located

138 downstream of the confluence between the upper WIS and Mercer Ice Stream (MIS), where the faster flow
139 of WIS relative to MIS leads to shear strain across the suture zone, which can reorientate ice crystals (see
140 Figure 4; Beem and others, 2014). However, Bindschadler and others (1987) argue that shear is minimal
141 between WIS and MIS. Additionally, we postulate that this suture zone has a negligible effect on the ice
142 COF at our study site because the significant mixing between the two ice streams in the suture zone would
143 perturb the ice fabric on length scales of the order of hundreds of metres. This mixing would likely yield
144 significant differences in the fast-polarisation S-wave azimuth (φ) between the different stations, yet the
145 fast-polarisation S-wave azimuths remain constant within uncertainty across the network (see Figure 1b)
146 and a dominant fast polarisation direction can be seen in Figure 3b. Nonetheless, even if our ice COF were
147 to be affected by this shearing, the suture zone is located upstream of our study site (see high strain rates
148 near the intersection of WIS and MIS in Figure 4) and therefore also supports the second hypothesis.

149 We instead favour the second hypothesis: that WIS has a “palaeo-COF” that preserves a record of WIS’
150 upstream palaeo-deformation. Ice core studies and numerical simulations suggest that such preservation
151 of a palaeo COF is possible (Faria, 2018; Llorens and others, 2022). This can be explained by the concept
152 of Microstructural Fading Memory, where polycrystalline ice temporarily inherits signatures from its past
153 microstructure that are progressively erased over a certain relaxation time (Faria, 2018). In the case of
154 WIS, this past microstructure is the remnant of upstream palaeo-deformation, such that the COF still
155 has not reoriented towards or re-equilibrated with the local principal compression direction. Most of the
156 ice deformation at WIP occurs along the shear margins (Truffer and Echelmeyer, 2003) and ice flow is
157 mainly accommodated by basal sliding, so internal deformation at Whillans is low but still existent. In
158 such flow regimes, lattice rotation plays an important role relative to dynamic recrystallisation in ice fabric
159 evolution (Azuma, 1994; Fan and others, 2021). The c-axes of the ice crystals always rotate towards the
160 principal direction of compression, which in ice streams is the azimuthal direction perpendicular to the flow
161 direction (Smith and others, 2017; Thorsteinsson and others, 2003). The meandering nature of WIS alters
162 the direction of compression, and therefore the ice COF, which we hypothesise in WIS evolves based on c-
163 axis rotation, represents an integrated history of upstream strain induced by this changing stress. As such,
164 it is difficult to pinpoint the origin of the fabric formation. However, for the ice COF to have developed
165 the observed oblique φ , part of the integrated strain history must have originated from upstream areas
166 in the ice stream where the flow direction was perpendicular to φ . Considering the present-day westward
167 flow direction only and fast S-wave polarisation uncertainties of 18°, these regions have a flow direction

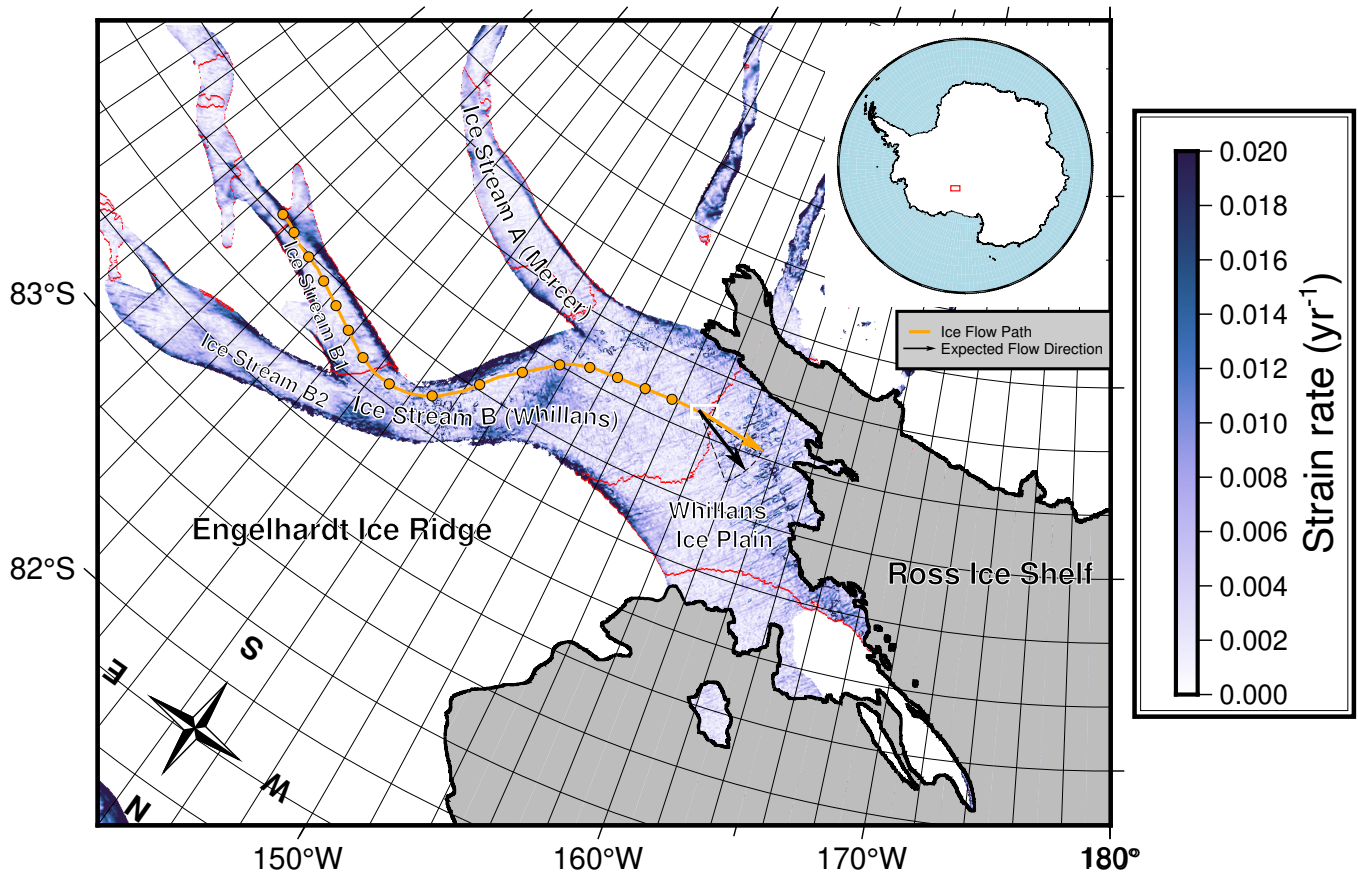


Fig. 4. A summary of the study findings. Regions with a flow direction between 281°N to 317°N , are shaded in red. The orange arrow shows the present-day flow direction. The black arrow indicates the flow direction inferred from the fast S-wave polarisation direction, and the dashed black sector outline shows the range of azimuths expressed by the red shaded regions. The background colour map is the strain rate calculated using the velocity map of Rignot and others (2017, supplementary information for calculation). Other features shown in this map are as in Figure 1a. The azimuth of the strain rate is shown in Figure S3.

168 approximately in the west-northwest direction of 281°N to 317°N (see shaded red regions in Figure 4).
169 The nearest region with such a flow direction along the ice flow path is in the southern tributary of WIS,
170 indicating that the ice COF could not have been purely derived from the integrated strain alone over the
171 past 450 years. Consequently, this implies that the entire ice stream flow field of WIS changes on timescales
172 shorter than ice COF re-equilibration. With this observation, we assumed constant flow directions with
173 time because ice-flow chronological studies do not suggest major changes in flow direction at WIS over the
174 past 500 years (Catania and others, 2012). Furthermore, the validity of this assumption does not affect our
175 conclusion of a palaeo-COF at WIS because present-day ice velocity orientations are insufficient to explain
176 the observed φ .

177 Larger strain rates can accelerate the rotation of lattices, which reduces the re-equilibration timescales
178 of ice fabrics and causes the COF to inherit signatures of the local strain field. Therefore, the integrated
179 strain history better preserves the fabric along flow where the strain is greater. From present-day velocities,
180 the largest strain rates are located on the main trunk of WIS before it merges with the MIS (see Figure
181 4). However, these strain rates could have been different in the past because of the dynamic nature of ice
182 streams. Some studies show that ice streams in the Ross Sea sector have variable mass fluxes over the
183 past centuries, in particular the Kamb Ice Stream (Bougamont and others, 2015; Catania and others, 2012;
184 Conway and others, 2002). Further studies of ice anisotropy, in combination with more detailed past ice
185 conditions and flow calculations, would further evidence any dynamic changes in ice anisotropy along WIS.

186 Given that the expected φ based on current ice flow is only just outside the uncertainty of our results,
187 we cannot ignore the possibility of an ice COF derived from the present-day study site. However, there
188 is only a negligible part of the study area that has a flow direction between 281°N and 317°N, with the
189 remainder of this region located downstream of the study site (see red shaded regions in Figure 4). Hence,
190 it is unlikely that enough time elapses for the ice COF to re-equilibrate with the present-day flow direction.
191 We therefore suggest that the ice fabric is most likely derived from upstream palaeo-deformation.

192 **Comparison to other COF studies at WIS**

193 Our results of an oblique fast S-wave direction (φ) differ from previous findings of an azimuth-independent
194 fabric (Picotti and others, 2015) and a fabric with φ parallel to flow between 170 m and 400 m depth
195 (Jordan and others, 2020). We attribute these differences to variations in sampling location and depth (see
196 Figure 1a).

197 Jordan and others (2020) find two types of vertical girdle fabrics at different depths: a fabric with φ
198 perpendicular to flow for ice up near the surface, and another fabric with φ parallel to flow up to 360 m deep.
199 The former fabric agrees with our results, while the latter suggests a longitudinally compressive instead
200 of longitudinally extensional stress regime, where compression and extension is defined as the principal
201 compression axis being parallel and perpendicular to flow respectively. Because their study was conducted
202 near the grounding line (see Figure 1a), we attribute the second girdle fabric (φ parallel to flow) to the
203 influence of longitudinal compression due to stronger interactions between the ice and the bed topography
204 near the grounding zone (Bindschadler and others, 1987; Picotti and others, 2015). If both fabrics are
205 present in the ice column at our study site, because we only invert for a single anisotropic layer, both
206 fabric orientations would then be represented as a single, composite result. If two perpendicular fabrics
207 are present, then any shear-wave splitting measurements would be unable to discriminate between the
208 layers, with the anisotropy amplitude (delay-time) being damped or amplified, but the overall orientation of
209 anisotropy remaining constant. Other studies have suggested that the stress regime at WIP is longitudinally
210 compressive (Bindschadler and others, 1987). However, this likely does not apply to our study site. Firstly,
211 the strain rates at WIS vary massively as little as 20 kilometres (see Figure 9 of Bindschadler and others,
212 1987). Secondly, the ice flow path inferred from present-day velocities indicates that the ice at our study site
213 has travelled along the outer part of the curve at WIP, where we expect the stress regime to be longitudinally
214 extensional (see Figure 4). Because most of the vertical shear needed to accommodate the driving stress
215 at WIS occurs within the basal sediment layer (MacAyeal, 1989), we expect the velocity orientation to
216 be similar across all depths of the ice stream. Thirdly, the ice at our study site is located sufficiently
217 far from the grounding line, such that it should not experience significant longitudinal compression from
218 interactions between the ice and grounding line bed topography (Pattyn, 2000).

219 Picotti and others (2015) observe an azimuth-independent fabric across the entire ice column, and
220 suggest that ice streams with low basal shear stress and highly-water-saturated sediments have COF
221 profiles similar to ice divides due to the increasing influence of vertical compression relative to transverse
222 compression. However, most of their study is based on surface wave data and travel-time inversions
223 that could only image the fabric up to 200 m at WIS. Furthermore, their study site is located above
224 Subglacial Lake Whillans, which is further inwards of the curve at WIP, where the stress regime is less
225 longitudinally extensional (see Figure 1a). Additionally, their ice COF is likely to have undergone more
226 equilibration caused by higher strain rates and lower flow velocities on the northern side of WIS (see Figure

227 4; Bindschadler and others, 1987). Given this variance in ice COF in WIS, future studies of ice deformation
228 and anisotropy can furthermore reveal the spatial and temporal variability of ice COF at WIS.

229 **Comparison to other ice streams**

230 Shear-wave splitting studies from another Antarctic ice stream, Rutford Ice Stream (RIS), find that the
231 COF at RIS is approximately perpendicular ($\sim 85^\circ$) to ice flow (Harland and others, 2013; Smith and others,
232 2017). Unlike the deviatoric nature of WIS stream flow, the flow direction at RIS is approximately linear
233 over COF re-equilibration timescales. As such, it is not possible to discriminate to what extent the COF
234 at RIS represents the current deformation or a preserved upstream deformation state. Kufner and others
235 (2023) suggest that the RIS COF signal is dominated by the latter. The strength of anisotropy, effectively
236 a measure of the strength of the ice COF, at RIS is 3-5 %, while that at WIS is 1.5 %, suggesting that
237 internal deformation is lower at WIS than RIS. This is consistent with findings that ice flow at WIS is
238 mainly accommodated by lateral shearing at the margins and basal sliding, where the vertical shear strain
239 rates required to support the driving stress are mostly confined within a weak basal till layer, and not
240 within the ice itself (Blankenship and others, 1986; MacAyeal, 1989; Truffer and Echelmeyer, 2003).

241 A recent seismic anisotropy study at RIS by Kufner and others (2023) suggested that multi-layer
242 anisotropy can be present in ice streams, where the deepest third of the ice stream is thought to comprise an
243 azimuthally isotropic cluster fabric caused by basal shearing (Azuma, 1994). However, the apparent absence
244 of multiple fast S-wave phase arrivals in our data suggests that the effects of any multi-layer anisotropy at
245 WIS are negligible, to which here we define multi-layer anisotropy as a type of depth-dependent anisotropy
246 with sharper changes in anisotropic signatures with depth. Indeed we did not observe sufficient hints of
247 multi-layer splitting to invert for multiple layers, even though such an inversion is possible at ice streams
248 (Hudson and others, 2023). Inverting for a multi-layer anisotropic model at WIS would introduce additional
249 parameters on layer thicknesses and fast polarisation directions, which could result in overfitting of the
250 data, compared to a single depth-integrated anisotropy model.

251 Because most of the vertical shear at WIS is accommodated within the basal sediment layer (MacAyeal,
252 1989), we would expect the surface velocity direction to represent the orientation of maximum strain with
253 depth, except perhaps for a thin (1 to 10s metres) basal shear layer near the ice-bed interface, which could
254 vary somewhat in orientation over short length scales (10s to 100s metres) due to local bed topography
255 variations. The depth of ice affected by shearing will either be too thin to be observed in seismic lengthscales

256 or too weak to affect the overall anisotropic signature of the ice stream (Bindschadler and others, 1987;
257 Blankenship and others, 1986). Additionally, even if the shear zone were to exhibit strong anisotropy, the
258 cluster fabric that would likely result is azimuthally isotropic and therefore has little effect on our results of
259 a preferred c-axis azimuth. In summary, we therefore would expect the dominant anisotropy to be oriented
260 relative to surface ice flow velocity.

261 **Implications of an oblique ice fabric on ice flow**

262 The effective viscosity for compression and extension is higher along the basal plane. As seen in RIS, where
263 the horizontal c-axis is oriented perpendicular to flow, the effective viscosity is higher along flow than across
264 flow (Jordan and others, 2022; Kufner and others, 2023). This hardening along the flow direction, which
265 is perpendicular to the c-axes and parallel to the basal plane, is thought to increase the viscosity by an
266 order of magnitude relative to isotropic ice (Kufner and others, 2023). However, our results at WIS show
267 a c-axis orientation that is not perpendicular, but oblique to ice flow or equivalently a misalignment of
268 the basal plane with the flow direction. Because the basal plane is associated with directions of highest
269 effective viscosity, this misalignment implies that internal deformation will be resisted more at WIS if the
270 c-axis direction re-equilibrates with the local principal stress direction. The internal deformation in WIS
271 might be minimal today, but it may become important in the future. Firstly, the long-term slowdown
272 in WIS has been associated with basal strengthening, especially in the upper portion of the ice stream
273 (Beem and others, 2014). If the driving stress is somehow sustained, then a lower proportion of this stress
274 could be accommodated by the basal till and a higher proportion through internal deformation. Secondly,
275 the deceleration results in increased duration between periods of slip events at WIS, which is expected to
276 increase the significance of internal viscous deformation (Winberry and others, 2014).

277 Our observations also suggest that palaeo ice COF can somewhat control present-day ice flow. If
278 the shape of an ice stream deviates on length scales less than the distance ice travels within the COF
279 re-equilibration time, then the COF may not be aligned with ice flow, limiting the effective viscosity of
280 the ice column along the ice flow direction. If an ice stream flows linearly for a duration greater than
281 the re-equilibration time, then the COF should re-equilibrate with the bulk stress, such that the basal
282 plane will rotate closer to the ice flow direction, increase the effective viscosity, and decrease the rate of
283 deformation downstream. The degree of re-equilibration of an ice COF with the surrounding stresses is
284 not only dependent on ice stream shape, but also on flow speed. Slower-flowing ice will have more time

285 to re-equilibrate with the surrounding stress field. The long-term slowdown at WIS can therefore provide
286 more time for its ice COF re-equilibration, which reduces the misalignment of the basal plane with flow
287 direction and increases the effective viscosity along the flow direction of WIS. Despite internal deformation
288 becoming more significant with the long-term slowdown, this higher effective viscosity instead indicates
289 that internal deformation will be more difficult, which has consequences on future predictions of the ice
290 flow at WIS.

291 Most icesheet-scale ice dynamics models assume either that ice is isotropic, or parameterise anisotropy
292 effects via an enhancement factor to account for ice weakening due to COF orientation relative to ice
293 flow. However, recent studies such as Smith and others (2017) and Kufner and others (2023), suggest that
294 enhancement factors should no longer be used to parameterise ice viscosity in fast-deforming regions such
295 as ice streams. Additionally, the effect of anisotropy on the viscosity of ice can differ significantly between
296 different types of ice fabrics. Most results concluding that ice weakens when anisotropy is considered
297 originate from studies based on cluster fabrics. Conversely, radar and seismic observations at RIS (Jordan
298 and others, 2022; Kufner and others, 2023), and numerical simulations (Ma and others, 2010) show that
299 ice with a girdle COF has a higher effective viscosity in relation to isotropic ice. Our findings at WIS
300 further support the importance of characterising COF- and directionally-dependent ice viscosity in ice flow
301 models, and emphasise that understanding ice COF in both space and time is important for producing
302 more realistic deformation in ice dynamics models.

303 CONCLUSION

304 This study provides shear-wave splitting (SWS) observations from basal icequakes at Whillans Ice Stream
305 (WIS). From these observations, we infer the ice crystal orientation fabric (COF) anisotropy over the entire
306 ice column. The observations provide insight into past and present deformation at WIS. The results from
307 80 discrete icequakes SWS observations show that WIS has an average fast S-wave direction (φ) of 29.3°,
308 which is oblique to the expected direction of $\sim 10^\circ$ based on ice flow direction at the study site of around
309 280°. We suggest that the ice COF records an integrated strain history along its flow path for at least the
310 past 450 years to have preserved deformation in the direction of φ , and therefore evidence the concept of
311 Microstructural Fading Memory. The non-perpendicularity of φ to ice flow implies that the shape of an
312 ice stream can affect its flow, such that spatially deviatoric ice streams including WIS can flow slower if
313 they were instead linear. Given the long-term slowdown of WIS, the basal plane will have more time to

314 re-equilibrate with the surrounding stress field, which can further contribute to the long-term slowdown.
315 Our results have implications for ice sheet models, suggesting that historic ice flow can preserve ice fabric
316 and hence directionally-dependent ice viscosity that might play an important role in such models.

317 SUPPLEMENTARY MATERIAL

318 The supplementary material for this article can be found at <https://doi.org/10.1017/jog.xxx>.

319 ACKNOWLEDGEMENTS

320 J.L. received funding from a NERC DTP Award (NE/S007474/1). T.S.H was funded by a Leverhulme Early
321 Career Fellowship (ECF-2022-499). We thank Alex Brisbourne for his comments, which have improved the
322 manuscript. For the purpose of Open Access, the authors have applied a CC BY public copyright licence
323 to any Author Accepted Manuscript (AAM) version arising from this submission.

324 **REFERENCES**

- 325 Azuma N (1994) A flow law for anisotropic ice and its application to ice sheets. *Earth and Planetary Science Letters*,
326 **128**(3-4), 601–614 (doi: 10.1016/0012-821X(94)90173-2)
- 327 Barcheck CG, Tulaczyk S, Schwartz SY, Walter JI and Winberry JP (2018) Implications of basal micro-earthquakes
328 and tremor for ice stream mechanics: Stick-slip basal sliding and till erosion. *Earth and Planetary Science Letters*,
329 **486**, 54–60 (doi: 10.1016/j.epsl.2017.12.046)
- 330 Barcheck CG, Schwartz SY and Tulaczyk S (2020) Icequake streaks linked to potential mega-scale glacial lineations
331 beneath an Antarctic ice stream. *Geology*, **48**(2), 99–102 (doi: 10.1130/G46626.1)
- 332 Barcheck G, Brodsky EE, Fulton PM, King MA, Siegfried MR and Tulaczyk S (2021) Migratory earthquake precursors
333 are dominant on an ice stream fault. *Science Advances*, **7**(6), eabd0105 (doi: 10.1126/sciadv.abd0105)
- 334 Beem LH, Tulaczyk SM, King MA, Bougamont M, Fricker HA and Christoffersen P (2014) Variable deceleration
335 of Whillans Ice Stream, West Antarctica. *Journal of Geophysical Research Earth Surf.*, **119**(2), 212–224 (doi:
336 10.1002/2013JF002958)
- 337 Bindschadler RA, Stephenson SN, MacAyeal DR and Shabtaie S (1987) Ice dynamics at the mouth of ice stream B,
338 Antarctica. *Journal of Geophysical Research*, **92**(B9), 8885 (doi: 10.1029/JB092iB09p08885)
- 339 Bindschadler RA, King MA, Alley RB, Anandakrishnan S and Padman L (2003) Tidally controlled stick-slip discharge
340 of a West Antarctic ice stream. *Science*, **301**(5636), 1087–1089 (<https://www.jstor.org/stable/3834979>)
- 341 Blankenship DD, Bentley CR, Rooney ST and Alley RB (1986) Seismic measurements reveal a saturated porous
342 layer beneath an active Antarctic ice stream. *Nature*, **322**(6074), 54–57 (doi: 10.1038/322054a0)
- 343 Bougamont M, Christoffersen P, Price SF, Fricker HA, Tulaczyk S and Carter SP (2015) Reactivation of Kamb Ice
344 Stream tributaries triggers century-scale reorganization of Siple Coast ice flow in West Antarctica. *Geophysical
345 Research Letters*, **42**(20), 8471–8480 (doi: 10.1002/2015GL065782)
- 346 Budd W and Jacka T (1989) A review of ice rheology for ice sheet modelling. *Cold Regions Science and Technology*,
347 **16**(2), 107–144 (doi: 10.1016/0165-232X(89)90014-1)
- 348 Catania G, Hulbe C, Conway H, Scambos T and Raymond C (2012) Variability in the mass flux of the
349 Ross ice streams, West Antarctica, over the last millennium. *Journal of Glaciology*, **58**(210), 741–752 (doi:
350 10.3189/2012JoG11J219)
- 351 Conway H, Catania G, Raymond CF, Gades AM, Scambos TA and Engelhardt H (2002) Switch of flow direction in
352 an Antarctic ice stream. *Nature*, **419**(6906), 465–467 (doi: 10.1038/nature01081)

- 353 Duval P, Ashby MF and Anderman I (1983) Rate-controlling processes in the creep of polycrystalline ice. *Journal of*
354 *Physical Chemistry*, **87**(21), 4066–4074 (doi: 10.1021/j100244a014)
- 355 Ester M, Kriegel HP, Sander J and Xu X (1996) A density-based algorithm for discovering clusters in large spatial
356 databases with noise. In *Proceedings of the Second International Conference on Knowledge Discovery and Data*
357 *Mining*, KDD’96, 226–231, AAAI Press, place: Portland, Oregon
- 358 Fan S, Cross AJ, Prior DJ, Goldsby DL, Hager TF, Negrini M and Qi C (2021) Crystallographic Preferred Orientation
359 (CPO) Development Governs Strain Weakening in Ice: Insights From High-Temperature Deformation Experiments.
360 *Journal of Geophysical Research: Solid Earth*, **126**(12), e2021JB023173 (doi: 10.1029/2021JB023173)
- 361 Faria SH (2018) Slip-band distributions and microstructural fading memory beneath the firn–ice transition of polar
362 ice sheets. *Mechanics Research Communications*, **94**, 95–101 (doi: 10.1016/j.mechrescom.2018.09.009)
- 363 Fricker HA and Scambos T (2009) Connected subglacial lake activity on lower Mercer and Whillans Ice Streams,
364 West Antarctica, 2003–2008. *Journal of Glaciology*, **55**(190), 303–315 (doi: 10.3189/002214309788608813)
- 365 Harland S, Kendall JM, Stuart G, Lloyd G, Baird A, Smith A, Pritchard H and Brisbourne A (2013) Deformation
366 in Rutford Ice Stream, West Antarctica: measuring shear-wave anisotropy from icequakes. *Annals of Glaciology*,
367 **54**(64), 105–114 (doi: 10.3189/2013AoG64A033)
- 368 Hudson TS, Brisbourne AM, Walter F, Gräff D, White RS and Smith AM (2020) Icequake Source Mechanisms
369 for Studying Glacial Sliding. *Journal of Geophysical Research: Earth Surface*, **125**(11), e2020JF005627 (doi:
370 10.1029/2020JF005627)
- 371 Hudson TS, Asplet J and Walker AM (2023) Automated shear-wave splitting analysis for single- and multi- layer
372 anisotropic media. *Seismica*, **2**(2) (doi: 10.26443/seismica.v2i2.1031)
- 373 Jordan TM, Schroeder DM, Elsworth CW and Siegfried MR (2020) Estimation of ice fabric within Whillans Ice Stream
374 using polarimetric phase-sensitive radar sounding. *Annals of Glaciology*, **61**(81), 74–83 (doi: 10.1017/aog.2020.6)
- 375 Jordan TM, Martín C, Brisbourne AM, Schroeder DM and Smith AM (2022) Radar Characterization of Ice Crystal
376 Orientation Fabric and Anisotropic Viscosity Within an Antarctic Ice Stream. *Journal of Geophysical Research:*
377 *Earth Surface*, **127**(6), e2022JF006673 (doi: 10.1029/2022JF006673)
- 378 Kufner S, Wookey J, Brisbourne AM, Martín C, Hudson TS, Kendall JM and Smith AM (2023) Strongly Depth-
379 Dependent Ice Fabric in a Fast-Flowing Antarctic Ice Stream Revealed With Icequake Observations. *Journal of*
380 *Geophysical Research: Earth Surface*, **128**(3), e2022JF006853 (doi: 10.1029/2022JF006853)
- 381 Lipenkov V, Barkov N, Duval P and Pimienta P (1989) Crystalline Texture of the 2083 m Ice Core at Vostok Station,
382 Antarctica. *Journal of Glaciology*, **35**(121), 392–398 (doi: 10.3189/S0022143000009321)

- 383 Llorens MG, Griera A, Bons PD, Weikusat I, Prior DJ, Gomez-Rivas E, De Riese T, Jimenez-Munt I, García-
384 Castellanos D and Lebensohn RA (2022) Can changes in deformation regimes be inferred from crystallographic
385 preferred orientations in polar ice? *The Cryosphere*, **16**(5), 2009–2024 (doi: 10.5194/tc-16-2009-2022)
- 386 Lomax A, Virieux J, Volant P and Berge-Thierry C (2000) Probabilistic Earthquake Location in 3D and Layered
387 Models. In CH Thurber and N Rabinowitz (eds.), *Advances in Seismic Event Location*, 101–134, Springer Nether-
388 lands, Dordrecht, ISBN 978-94-015-9536-0 (doi: 10.1007/978-94-015-9536-0_5)
- 389 Lutz F, Eccles J, Prior DJ, Craw L, Fan S, Hulbe C, Forbes M, Still H, Pyne A and Mandeno D (2020) Constraining
390 Ice Shelf Anisotropy Using Shear Wave Splitting Measurements from Active-Source Borehole Seismics. *Journal of*
391 *Geophysical Research: Earth Surface*, **125**(9), e2020JF005707 (doi: 10.1029/2020JF005707)
- 392 Ma Y, Gagliardini O, Ritz C, Gillet-Chaulet F, Durand G and Montagnat M (2010) Enhancement factors for
393 grounded ice and ice shelves inferred from an anisotropic ice-flow model. *Journal of Glaciology*, **56**(199), 805–812
394 (doi: 10.3189/002214310794457209)
- 395 MacAyeal DR (1989) Large-scale ice flow over a viscous basal sediment: Theory and application to ice stream B,
396 Antarctica. *Journal of Geophysical Research*, **94**(B4), 4071–4087 (doi: 10.1029/JB094iB04p04071)
- 397 Menke W and Levin V (2003) The cross-convolution method for interpreting *SKS* splitting observations, with ap-
398 plication to one and two-layer anisotropic earth models. *Geophysical Journal International*, **154**(2), 379–392 (doi:
399 10.1046/j.1365-246X.2003.01937.x)
- 400 Morgan V, Jacka T, Akerman G and Clarke A (1982) Outlet Glacier and Mass-Budget Studies in Enderby, Kemp,
401 and Mac. Robertson Lands, Antarctica. *Annals of Glaciology*, **3**, 204–210 (doi: 10.3189/S0260305500002780)
- 402 Morlighem M (2022) MEaSUREs BedMachine Antarctica, Version 3 (doi: 10.5067/FPSU0V1MWUB6)
- 403 Pattyn F (2000) Ice-sheet modelling at different spatial resolutions: focus on the grounding zone. *Annals of Glaciology*,
404 **31**, 211–216 (doi: 10.3189/172756400781820435)
- 405 Picotti S, Vuan A, Carcione JM, Horgan HJ and Anandakrishnan S (2015) Anisotropy and crystalline fabric of
406 Whillans Ice Stream (West Antarctica) inferred from multicomponent seismic data. *Journal of Geophysical Re-*
407 *search: Solid Earth*, **120**(6), 4237–4262 (doi: 10.1002/2014JB011591)
- 408 Pimienta P, Duval P and Lipenkov VY (1987) Mechanical behavior of anisotropic polar ice. In *Proceedings of the*
409 *Vancouver Symposium*, volume 170, 57–66, International Association of Hydrological Sciences
- 410 Pratt MJ, Winberry JP, Wiens DA, Anandakrishnan S and Alley RB (2014) Seismic and geodetic evidence for
411 grounding-line control of Whillans Ice Stream stick-slip events: Whillans Ice Stream Stick-Slip Events. *Journal of*
412 *Geophysical Research Earth Surface*, **119**(2), 333–348 (doi: 10.1002/2013JF002842)

- 413 Rignot E, Mouginot J, Morlighem M and Scheuchl B (2017) MEaSUREs InSAR-Based Antarctica Ice Velocity Map,
414 Version 2 (doi: 10.5067/D7GK8F5J8M8R)
- 415 Schwartz SY (2012) Whillans Ice Stream Subglacial Access Research Drilling (doi: 10.7914/SN/YD_2012)
- 416 Siegfried MR, Fricker HA, Carter SP and Tulaczyk S (2016) Episodic ice velocity fluctuations triggered by a subglacial
417 flood in West Antarctica. *Geophysical Research Letters*, **43**(6), 2640–2648 (doi: 10.1002/2016GL067758)
- 418 Smith EC, Baird AF, Kendall JM, Martín C, White RS, Brisbourne AM and Smith AM (2017) Ice fabric in an
419 Antarctic ice stream interpreted from seismic anisotropy. *Geophysical Research Letters*, **44**(8), 3710–3718 (doi:
420 10.1002/2016GL072093)
- 421 Teanby NA, Kenda NA, Kendall JM, Martin C, White RS, Brisbourne AM and Smith AM (2004) Automation
422 of Shear-Wave Splitting Measurements using Cluster Analysis. *Bulletin of the Seismological Society of America*,
423 **94**(2), 453–463 (doi: 10.1785/0120030123)
- 424 Thorsteinsson T, Waddington ED and Fletcher RC (2003) Spatial and temporal scales of anisotropic effects in
425 ice-sheet flow. *Annals of Glaciology*, **37**, 40–48 (doi: 10.3189/172756403781815429)
- 426 Truffer M and Echelmeyer KA (2003) Of isbræ and ice streams. *Annals of Glaciology*, **36**, 66–72 (doi:
427 10.3189/172756403781816347)
- 428 Walsh E, Arnold R and Savage MK (2013) Silver and Chan revisited. *Journal of Geophysical Research: Solid Earth*,
429 **118**(10), 5500–5515 (doi: 10.1002/jgrb.50386)
- 430 Walter JI, Brodsky EE, Tulaczyk S, Schwartz SY and Pettersson R (2011) Transient slip events from near-field
431 seismic and geodetic data on a glacier fault, Whillans Ice Plain, West Antarctica. *Journal of Geophysical Research*,
432 **116**(F1), F01021 (doi: 10.1029/2010JF001754)
- 433 Walter JI, Svetlizky I, Fineberg J, Brodsky EE, Tulaczyk S, Grace Barcheck C and Carter SP (2015) Rupture speed
434 dependence on initial stress profiles: Insights from glacier and laboratory stick-slip. *Earth and Planetary Science*
435 *Letters*, **411**, 112–120 (doi: 10.1016/j.epsl.2014.11.025)
- 436 Wang Y, Thorsteinsson T, Kipfstuhl J, Miller H, Dahl-Jensen D and Shoji H (2002) A vertical girdle fabric in the
437 NorthGRIP deep ice core, North Greenland. *Annals of Glaciology*, **35**, 515–520 (doi: 10.3189/172756402781817301)
- 438 Weikusat I, Jansen D, Binder T, Eichler J, Faria SH, Wilhelms F, Kipfstuhl S, Sheldon S, Miller H, Dahl-Jensen D and
439 Kleiner T (2017) Physical analysis of an Antarctic ice core—towards an integration of micro- and macrodynamics
440 of polar ice. *Philosophical Transactions of the Royal Society A*, **375**(2086), 20150347 (doi: 10.1098/rsta.2015.0347)

- 441 Winberry JP, Anandakrishnan S, Alley RB, Bindschadler RA and King MA (2009) Basal mechanics of ice streams:
442 Insights from the stick-slip motion of Whillans Ice Stream, West Antarctica. *Journal of Geophysical Research*,
443 **114**(F1), F01016 (doi: 10.1029/2008JF001035)
- 444 Winberry JP, Anandakrishnan S, Wiens DA, Alley RB and Christianson K (2011) Dynamics of stick-slip
445 motion, Whillans Ice Stream, Antarctica. *Earth and Planetary Science Letters*, **305**(3-4), 283–289 (doi:
446 10.1016/j.epsl.2011.02.052)
- 447 Winberry JP, Anandakrishnan S, Wiens DA and Alley RB (2013) Nucleation and seismic tremor associated with
448 the glacial earthquakes of Whillans Ice Stream, Antarctica. *Geophysical Research Letters*, **40**(2), 312–315 (doi:
449 10.1002/grl.50130)
- 450 Winberry JP, Anandakrishnan S, Alley RB, Wiens DA and Pratt MJ (2014) Tidal pacing, skipped slips and the slow-
451 down of Whillans Ice Stream, Antarctica. *Journal of Glaciology*, **60**(222), 795–807 (doi: 10.3189/2014JoG14J038)
- 452 Wuestefeld A, Al-Harrasi O, Verdon JP, Wookey J and Kendall JM (2010) A strategy for automated analysis of passive
453 microseismic data to image seismic anisotropy and fracture characteristics: A strategy for automated analysis of
454 passive microseismic data. *Geophysical Prospecting*, **58**(5), 755–773 (doi: 10.1111/j.1365-2478.2010.00891.x)